npg

ORIGINAL ARTICLE

Resistive–conductive transitions in the time-dependent piezoresponse of PVDF-MWCNT nanocomposites

Shailesh Vidhate[1], Jaycee Chung[2], Vijay Vaidyanathan[1] and Nandika Anne D'Souza[1]

Nanocomposites were prepared by melt blending of multiwalled carbon nanotubes (MWCNTs) filled with polyvinylidene fluoride. Time-dependent piezoresistance was investigated as a function of concentration. In the quasi-static case, a transition from negative pressure coefficient to positive pressure coefficient (PPC) behavior was observed. The PPC effect was negligible at high concentrations. At short times, the resistive response decreased for all nanocomposites, with the magnitude of the decrease proportionate to the MWCNT concentration. However, long-term creep response was resistive for low concentrations and conductive at high concentrations. A Burgers model based on Maxwell and Kelvin elements in series was used to describe the strain dependence. An equivalent model that uses resistances and capacitances was examined for the time dependence of fractional resisitivity. Results were correlated with Raman mapping-based dispersion analysis. An increased dispersion and an increase in MWCNT–MWCNT contact area resulted in a transition from a matrix-based resistive response to a filler-based conductive response.

INTRODUCTION

Piezoresistivity is a phenomenon in which the electrical resistance of a material changes with an applied stress or strain. This phenomenon can be used to make sensors that monitor the change in stress or strain on a material by analyzing the electrical response of the material. Many researchers are applying this phenomenon using various materials systems with a range of electrically conductive fillers. The materials systems, which are being investigated in this study, are thermoplastics,[1–12] thermoset resins,[13,14] and cement.[15] Of the various types of nanofillers, carbon nanotubes (CNTs) are the dominant choice when conductivity is necessary, because they provide high strength and modulus at low concentration.[1,16]

If polymer-CNT composites can be used for strain sensing, then conventional expensive electronic sensors are not necessary. Polymer-CNT composites are also easy to prepare using melt blending-based techniques such as extrusion and injection molding. The ease of processing and low concentrations of multiwalled CNTs (MWCNTs) needed for enhanced mechanical and electrical response indicate that reduced cost, good mechanical strength and ease of strain monitoring can be realized. The piezoresistive effect can be used to develop various strain sensors or self-sensing composite structures and some mechanical damage-based self-monitoring materials.[2–5,13,17,18]

By incorporating CNTs, multifunctional mechanical and electrical response is facilitated. Increases in mechanical strength and electrical conductivity are simultaneously obtained.[6–10,19] Polymer-CNT composites have attracted considerable scientific and commercial interest because they show unique electrical and mechanical properties, in addition to some properties that are similar to the properties of polymeric materials, such as low weight, low cost, easy processing and corrosion resistance. When mechanical force is applied to MWCNT composites, changes in nanotube concentration affect the measured resistivity. Changes in the resistance of conductive composites are mainly due to the change in the interparticle separation distance. Any process that can change the particle-to-particle distance can change the resistivity response. For example, the application of stress on a filled system can change the particle-to-particle distance. Depending on the filler concentration loading level, time- and stress-dependent changes can be observed. The increase in resistance with increases in pressure is called a positive pressure coefficient (PPC) phenomenon, and the opposite is called a negative pressure coefficient (NPC) phenomenon.

Several papers have been published on the study of various aspects related to the piezoresitivity of polymer and conducting filler composites. The main reason for piezoresistance is differences in the compressibility of matrix and filler constituents, material composition, load content and filler content.[11] When the concentration of the filler content is increased, the resistance of the material slowly decreases to the percolation threshold and then decreases rapidly until the

conducting particles come in close contact with each other. Once the conducting particles come in close contact, the resistance remains constant at very high filler concentration.[12,14,20,21]

Mechanical strain due to tensile or compressive stress also causes a change in resistance.[22–25]

In this study, experimental results for polyvinylidene fluoride (PVDF)/MWCNT conductive composites are demonstrated. Previous research on PVDF/MWCNT composites showed various outstanding properties such as a low percolation threshold for electrical conductivity,[26] improved piezoresitivity,[27] improved strain-sensing ability,[28] good interfacial adhesion between nanotubes and PVDF[29] and improved crystallinity.[11] There are very few reports on the time-dependent piezoresistive behavior of conducting composites. For HDPE/short carbon fiber conductive composites, Zheng et al.[30] suggested that the molecular motion of the matrix due to creep causes local rearrangement of the percolation network, which leads to resistance creep and resistance relaxation. In another paper, Chen et al.[31] worked on HDPE/graphite composites and demonstrated the presence of critical stress. Above the critical stress, resistivity increases with time. Below the critical stress, resistivity decreases with time.

Although several research attempts have been made to understand the piezoresistive behavior of the conducting material, the following questions remain: (a) How does the concentration of the conducting filler affect the time-dependent behavior of the material? (b) How can the time-dependent behavior be predicted on the basis of a mathematical model? Herein, the piezoresistive behavior of the conductive composites is studied with compression and creep tests using various concentrations of fillers. An analogy between electrical and mechanical laws[32] is used to generate a model to predict time-dependent piezoresistivity with respect to deformation and fractional resistance response.

Burgers model

The classic way to derive viscoelastic constitutive models is by using mechanical analogs. These are simple mechanical models for fluid and solid representations that are put together to produce viscoelastic effects. The simplest mechanical analog for a linear elastic material is a spring. The simple constitutive relationship for a spring relates the force (stress when force is divided by area) to elongation or displacement (strain when displacement is normalized by length of the spring)

$$\sigma = E\varepsilon \tag{1}$$

where σ is the applied stress, E is the elastic modulus and ε represents the resultant strain.

The mechanical analog for a Newtonian fluid is a dashpot. The simple constitutive relationship for a dashpot indicates that the force in the fluid depends on the rate at which the dashpot is displaced

or, equivalently, the velocity of the dashpot. The constitutive parameter that relates force (stress) to displacement rate (strain rate) is viscosity η.

$$\sigma = \eta \frac{d\varepsilon}{dt} = \eta\dot{\varepsilon} \tag{2}$$

The Burgers model is a theoretical model that uses a combination of springs and dashpots connected in a series and parallel arrangement to describe the viscoelastic macroscopic behavior of materials.[33] The total strain is the sum of elastic and viscous strains. The total strain is given by

$$\varepsilon = \sigma/E_M + \sigma/E_K[1 - \exp(-E_K t/\eta_K)] + \sigma t/\eta_M \tag{3}$$

As shown in Figure 1, when stress σ is applied, the Maxwell spring E_M initially deforms. The Kelvin spring E_K and the dashpot η_K show a delayed deformation at longer times. When the applied force is removed (recovery), the Maxwell spring recovers completely. The Kelvin spring and the dashpot show delayed deformation.

The electrical analogy is obtained by making stress σ equivalent to the electric current I; strain ε is equivalent to the electric potential V; the material modulus E is equivalent to conductance Y; the viscosity parameter η is equivalent to the capacitor characteristic C. Thus, we obtain

$$\frac{\Delta R}{R_0} = \frac{I_0}{Y_M} + \frac{I_0}{Y_K}(1e^{t/\tau}) + \frac{I_0}{C_M}t; \; \tau = \frac{C_k}{Y_K}$$

EXPERIMENTAL PROCEDURE

Materials

PVDF was supplied by Arkema (Philadelphia, PA, USA) (Kynar 721, powder form) with the following properties: density, $1.78\,g\,cc^{-1}$; MFI, 10 g per 10 min; tensile strength, 54 MPa; and melting temperature, 168 °C. MWCNTs (Baytubes C150 P) were obtained from Bayer Material Science (Leverkusen, Germany), with the outer number of walls between 3 and 15, an outer mean diameter of 13–16 nm, an inner mean diameter of 4 nm, a length of 1–10 mm and a bulk density of $140–160\,kg\,m^{-3}$. MWCNT were used as received without further purification. Before melt mixing, both materials were vacuum dried at 150 °C for 1 h. PVDF and MWCNT were dry mixed by tumbling in a bottle. The contents of MWCNT in PVDF powder were 0, 1, 2, 4 and 10% by weight, and the compositions were coded as PVDF, PVDFCNT1, PVDFCNT2, PVDFCNT4 and PVDFCNT10, respectively.

Sample preparation

MWCNT and PVDF were melt blended in a twin screw extruder at 230 °C and 200 r.p.m., followed by compression molding at 220 °C under 10 MPa for 10 min to form a sheet with a smooth surface. After being cooled naturally to room temperature, the sheet was cut into samples with a size of $25 \times 25 \times 3\,mm^3$. Silver paste and copper mesh were mounted on both surfaces to ensure good electrical contact. All experiments were conducted in triplicate.
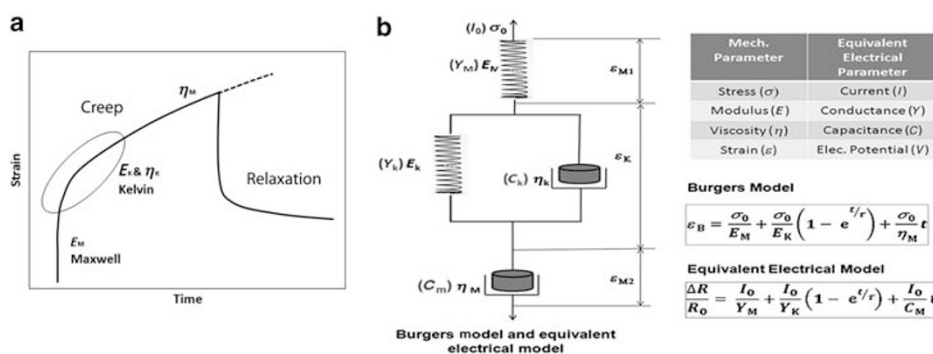

Figure 1 (**a**) A typical creep relaxation curve for a viscoelastic material. (**b**) Schematic diagram of the Burgers model and the equivalent electric model.
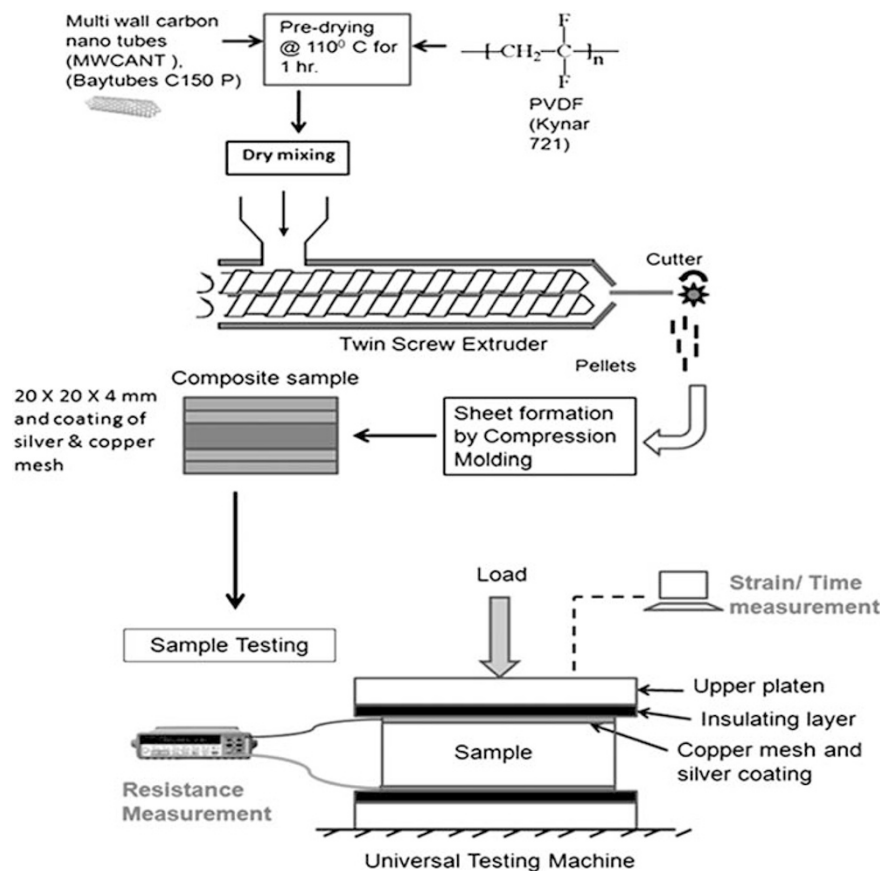
Figure 2 Experimental procedure showing the sample preparation method and electrical and mechanical response measurement techniques.
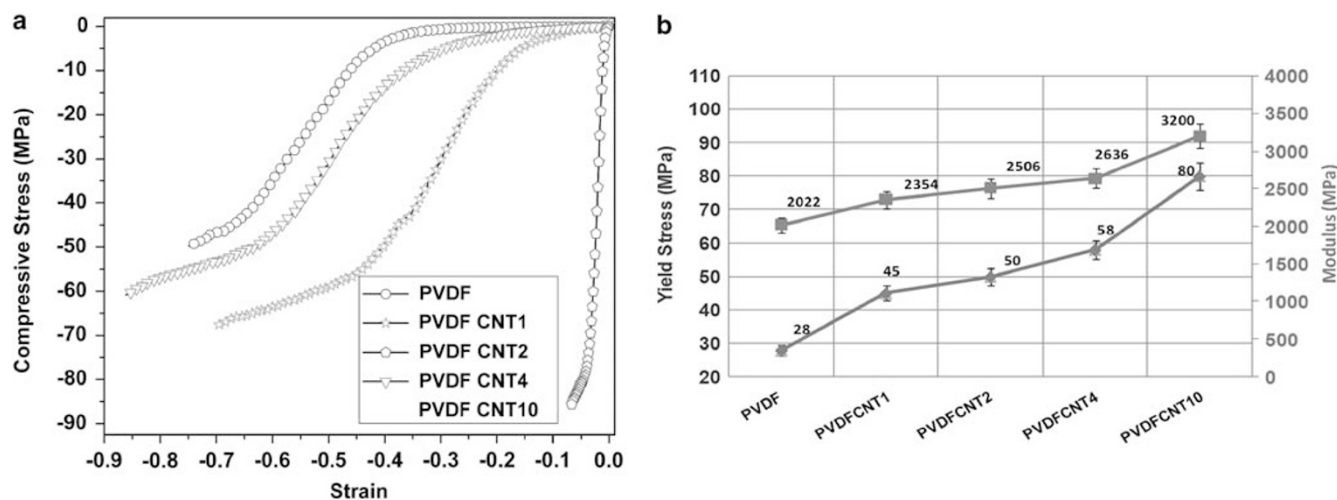

Figure 3 (**a**) Compressive stress strain curves. (**b**) Yield stress and compressive modulus values comparison for PVDF/MWCNT composites.

Measurements

Compression tests were performed on an MTS 810 Material Test System (MTS, Eden Prairie, MN, USA), universal testing machine, in which the bottom platen was fixed and the upper platen was only mobile along the uniaxial direction. The two-probe method was used to measure volume resistance using an Agilent 34410A multimeter (Agilent Technologies, Santa Clara, CA, USA). The two-probe method is based on Ohm's law: $V = IR$, with V, I and R indicating the voltage, current and resistance between the two electrodes, respectively. As the difference between the resistivity of the copper electrode and the material

was significant, a two-point over four-point measurement configuration was found to be equitable. When an electrical multimeter is connected to the two ends of the conductive wires, a circuit is formed through a conductive composite sample, and a direct current is produced by the power of the meter. Resistance was measured using Ohm's law based on current and voltage.

The experimental setup for simultaneous measurements of stress, strain and volume resistance is schematically illustrated in Figure 2. For each creep test, the specimen was compressed with a certain axial constant stress, which was maintained during the creep period. During relaxation, the stressed sample was

unloaded to zero force and strain was monitored during the recovery period. Compression tests were conducted at a speed of 0.5 mm min^{-1}. The axial compressive force and displacement data were automatically recorded using a computer. Engineering stress was determined as the ratio of axial force to the cross-sectional area of the specimen, and compression stain was defined as $\varepsilon = \frac{l_0 - l}{l_0} \times 100\%$, where l is the deformed length at time t. For creep tests, l_0 is the axial length of the composite at the beginning of the creep process, and ε represents the creep strain. Compressive creep tests for all samples were performed under constant stress below the maximum yield stress of the sample.

Raman spectroscopy

For recording Raman spectra, film samples of all compositions were used. All Raman spectra were recorded on an Almega XR Dispersive Raman spectrometer (Thermo Nicolet, Madison, WI, USA) equipped with a microscope, using a 20-fold magnification objective, by co-adding four spectra with collection times of 10 s each. An argon ion laser with a wavelength of 514 nm was used. Multiple grating that provides a resolution starting from 1000 to 2800 cm^{-1} for the argon ion laser was used. The abscissa was calibrated with the 520.7 cm^{-1} peak of a silicon standard, and the sharp Raman shifts were accurate within the limits of the resolution. To eliminate the influence of experimental parameters, all compositions were measured on the same day.

RESULTS AND DISCUSSION

Compression test

Compression tests were performed to determine the maximum yield stress value for the sample. The compression test results for all compositions are shown in Figures 3a and b. It is clear that with an increase in MWCNT content in PVDF, compressive yield stress and modulus values increase. Yield stress values for PVDF, PVDFCNT1, PVDFCNT2, PVDFCNT4 and PVDFCNT10 were 28, 45, 50, 58 and 80 MPa, respectively.

As shown in Figure 4, at various weight % of MWCNT concentrations (although prominently in 1 and 2% MWCNT composites,
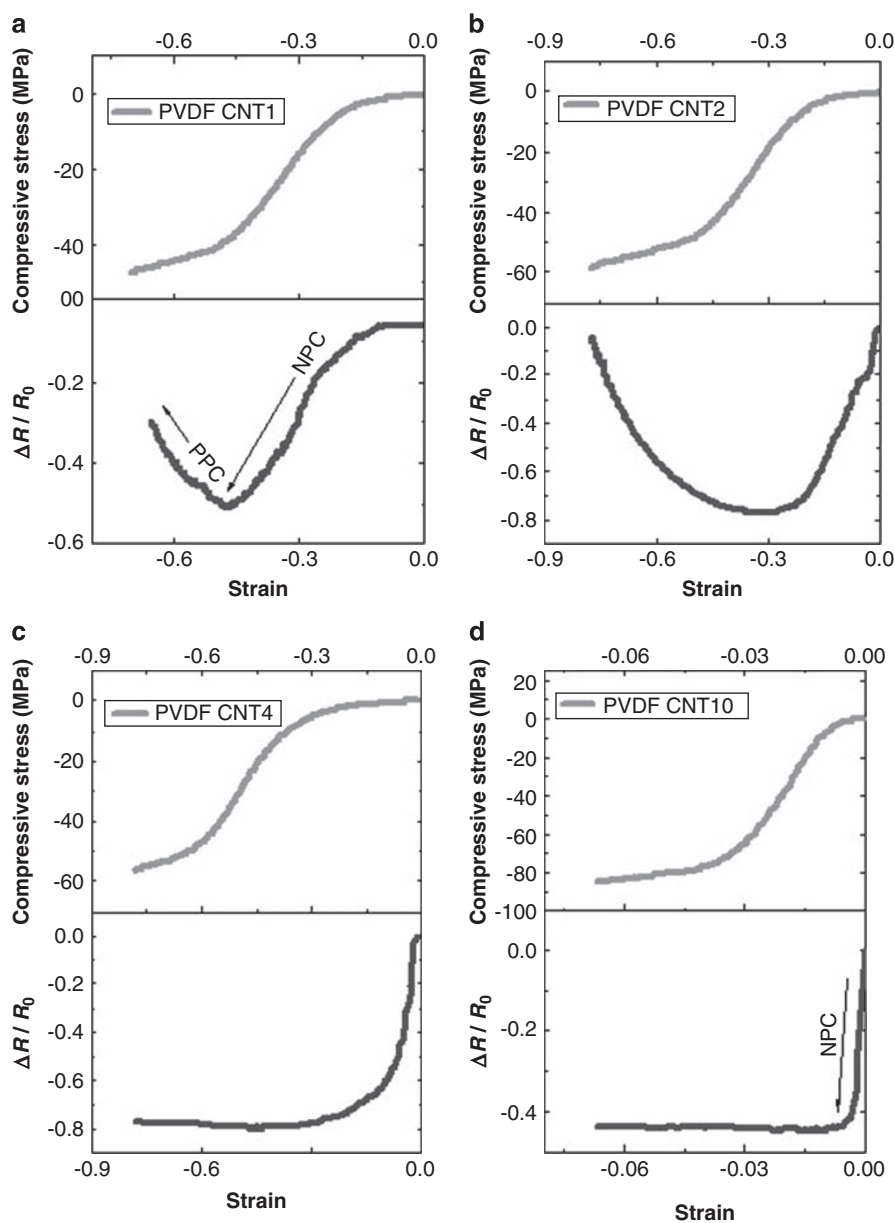

Figure 4 Resistance change as a function of applied pressure in piezoresistive composites. The presence of PPC and NPC phenomena in (a) PVDFCNT1 and (b) PVDFCNT2. (c) PVDFCNT4 and (d) PVDFCNT10 showing only NPC behavior.

Figures 4a and b) under compressive stress, both PPC and NPC phenomena were observed. In Figure 4, R_0 is the resistance before loading and R is the resistance under the loading condition. In the composites, MWCNT can be considered as incompressible, as Young's modulus of MWCNT is considerable (0.9–5.5 TPa).[33] When the composite is compressed, the compressibility of the matrix leads to a decrease in the interparticle distance of the MWCNT. Close conducting paths can decrease the resistance of the composite, that leads to the NPC effect. Further compression above the yield stress results in plastic deformation. The plastic deformation may cause MWCNT slippage and an increase in interparticle distance. In addition, at compressive stresses above the yield stress, the orientation of MWCNT in the transverse direction, buckling or breakdown of MWCNT and the destruction of the conducting path formed by MWCNT result in an increased resistance of the sample at strains greater than the yield strain. Thus, mechanisms that result in breaking the MWCNT–MWCNT contact result in PPC behavior. With a higher concentration of MWCNT (4 and 10%), the increased concentration leads to increased particle contact. Thus, the slippage or realignment of MWCNT does not influence the particle-to-particle distance and little to no PPC behavior is evident (Figures 4c and d).

Resistance response for creep and relaxation of PVDF/MWCNT composites

Transient tests were performed using the method of Fotheringham and Cherry,[34] which involves stressing a sample and then immediately removing the applied stress and allowing the sample to relax at zero stress. The specimens were loaded using a mechanical test system with a stress ramp-up rate of 0.5 MPa min^{-1}. When the sample reached a

Figure 5 Experimental and predicted creep compliance versus time curves.

predetermined value of stress, namely 20 MPa, the stress was maintained for 1 h. The strain was monitored for 1 h during the period of constant load application (creep segment), as well as for an hour after the release of the constant load (recovery segment). Creep compliance was calculated by dividing the obtained strain values by a constant stress. All tests were performed at an ambient temperature. Figure 5 shows the effect of sample composition on creep compliance. With an increase in filler concentration, creep compliance decreased. It can be seen that at higher percentage of MWCNT concentrations, higher elasticity in the material causes relaxation to occur faster than in the lower percentage of MWCNT-filled samples. The fitting parameters that correspond to the mechanical response are shown in Table 1. From the mechanical fits, we deduce that the Maxwell initial elastic response trends are similar to the quasi-static elastic modulus (Figure 3b). The short-term time dependence that corresponds to the Kelvin element shows similar trends for both elastic and viscous response versus concentration. Long-term constant rate viscosities also increased with concentration.

Similar to PPC and NPC, two new phenomena were observed by changing the concentration of filler weight % in the PVDF matrix. At low weight % (1 and 2) of MWCNT, the observed resistance increased with time, and the opposite phenomenon was observed at high weight % (4 and 10) concentration of MWCNT. The corresponding resistance curves are shown in Figure 6b. The initial resistance response is always conductive, but time-dependent behavior leads to a concentration-dependent resistive/conductive response that depends on the MWNCT concentration. At low concentrations, less particle-to-particle contact is expected. With the applied compressive stress, particles are pushed and the interparticle distance decreases. Thus, resistivity initially decreases, but the time-dependent phenomenon is more influenced by the polymer that is constrained between the conductive MWCNTs. The corresponding fitting parameters show the conductivity of the instantaneous response. Elements corresponding to the Kelvin time-dependent segment (Table 1) indicate a negative capacitance. Negative capacitances are reportedly due to charge injection in mixtures of materials with differences in resistivity of the constituents, or they are due to the release of charges that are trapped at the interface.[35] It is noted that the electrical resistance of MWCNT is far less than that of the PVDF matrix. At high concentrations, the gap between MWCNT particles is small enough for tunneling to occur. The small gap leads to the formation of local conductive pathways. This tunneling effect has been associated with negative capacitances in semiconductor–conductor mixtures. The time-dependent polymer relaxation resulted in an increased interparticle distance and a long-term capacitive/resistive response.

At higher concentrations, the increased interparticle contact results in a conductive material and a resistive/capacitive initial response. In the long term, the charge injection, because of the applied current, leads to the formation of electrets and negative capacitances toward the end of the test.
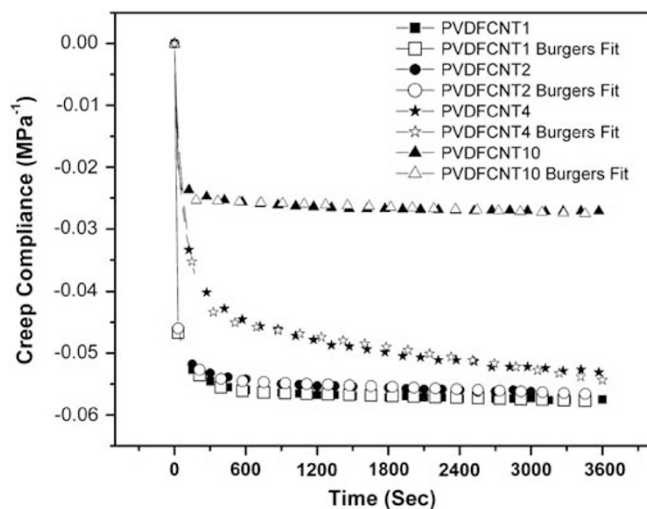
Table 1 Results for electrical fit

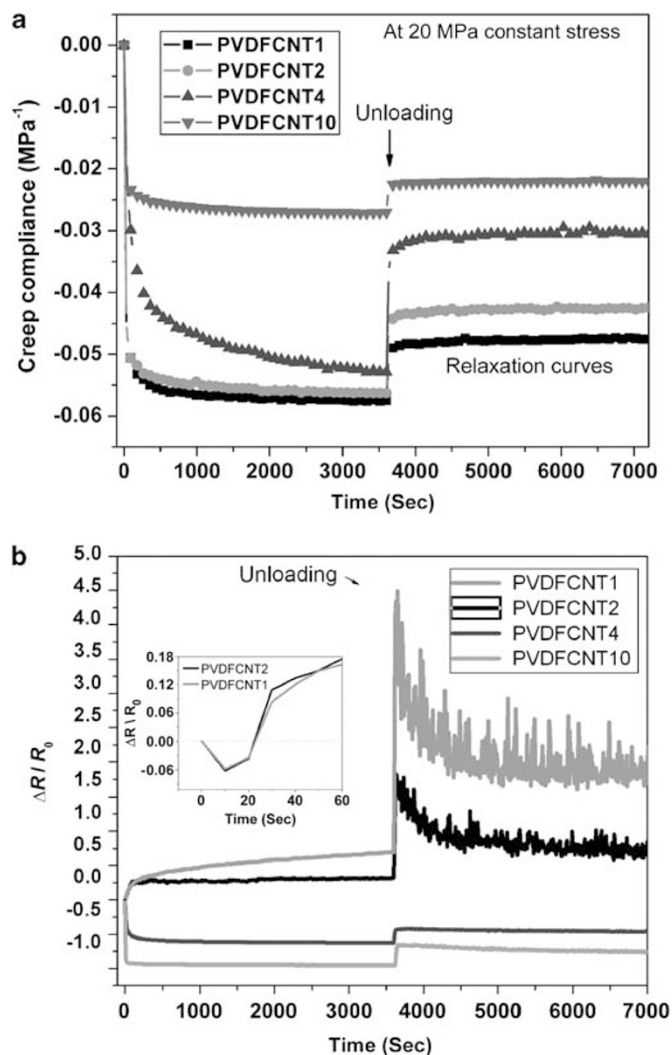| Sample	E_M (MPa)	E_K (MPa)	η_M (Gpa h)	η_K (Gpa h)	$\tau = \eta_K/E_K$	Y_m (S)	Y_k (S)	C_m (µF)	C_k (µF)	$\tau_{R=Ck/Ym}$
PVDF	3509	8320	746	180	21.6					
PVDFCNT1	3470	12320	945	324	26.3	9.8	3.4	11700	−881	−261.7
PVDFCNT2	3643	13276	875	360	27.1	19.5	3.2	59500	−135	−41.8
PVDFCNT4	3821	16982	1284	456	26.9	3.4	3.3	−88200	221	66.6
PVDFCNT10	4264	20876	1394	532	25.5	4429.5	1.1	−232000	4.4	4.1

Figure 6 (a) Creep compliance versus time curves and (b) simultaneously recorded change in resistance versus time curves of PVDF/MWCNT composites.
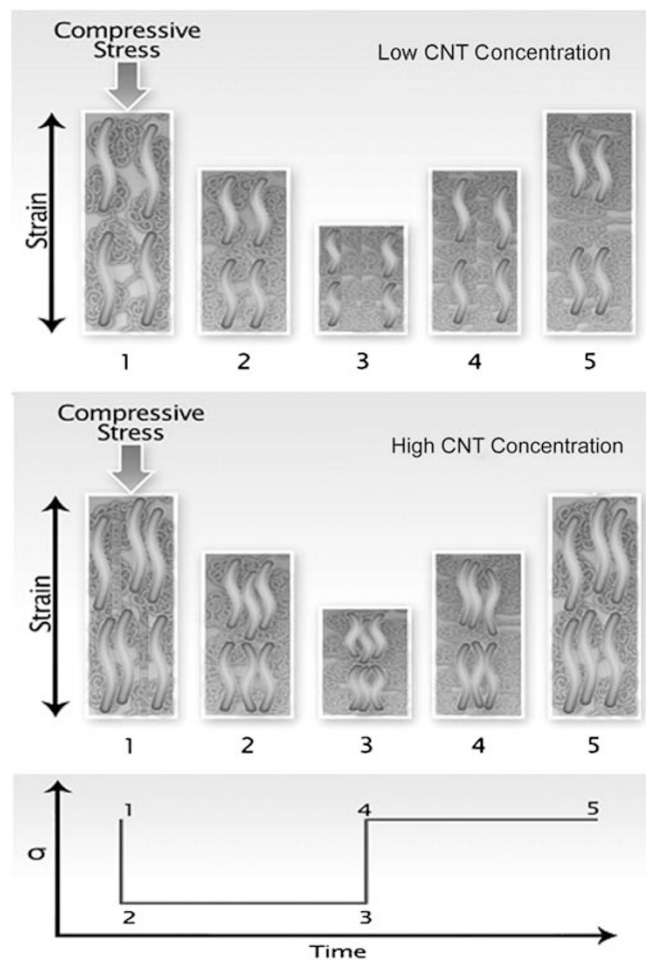

Figure 7 Schematic showing the effect of the MWCNT–MWCNT contact that leads to a time-dependent resistive response at low concentrations and a conductive response at high concentrations.

During recovery following creep, when all stress is removed, a sudden increase in resistance was observed at both high and low CNT concentrations. This corresponds to the instantaneous response of the polymer. At low concentrations, in which resistivity is dominant, the remnant resistivity remains relatively time independent with low time dependence. This indicates that the lack of particle-to-particle contact is responsible for remnant resistance. Resistive response persists when the load is removed, and particle-to-particle distances are relatively unchanged as the material recovers. At higher concentrations, the interparticle distances that were shortened during the application of compressive loads and coupled to increased filler–filler contact caused an increase in conductivity. Dimensional recovery results in an increase in junction distances, causing an increase in resistivity. With time, polymer recovery led to a gradual relaxation of the polymer matrix, causing a decrease in resistivity as the material approached the architecture that was present before the application of stress. The difference between low and high concentrations is shown in the schematic in Figure 7. At low concentrations, under the applied stress, the matrix between nanotubes was the active piezoresponsive element. There were fewer MWCNT–MWCNT contacts, and the response was largely resistive. At higher concentrations, more
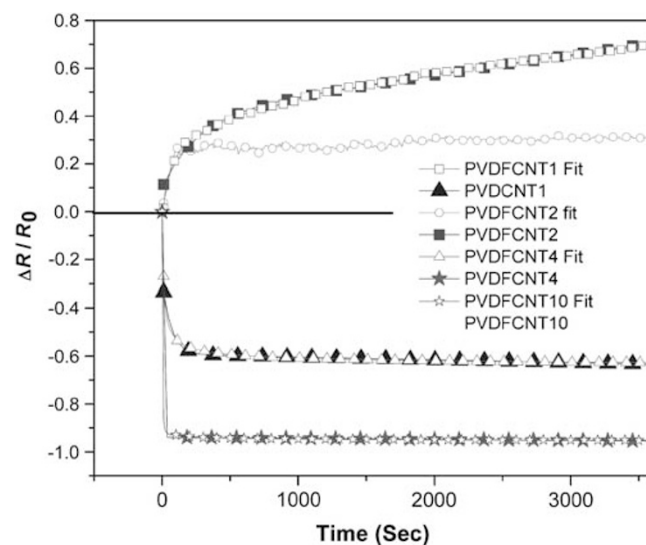

Figure 8 Experimental and predicted resistance creep versus time curves.

MWCNT–MWCNT contact led to a conductive response. The fitted results for the electrical analogy are shown in Figure 8. The schematic of the transition from resistive to conductive response was replicated
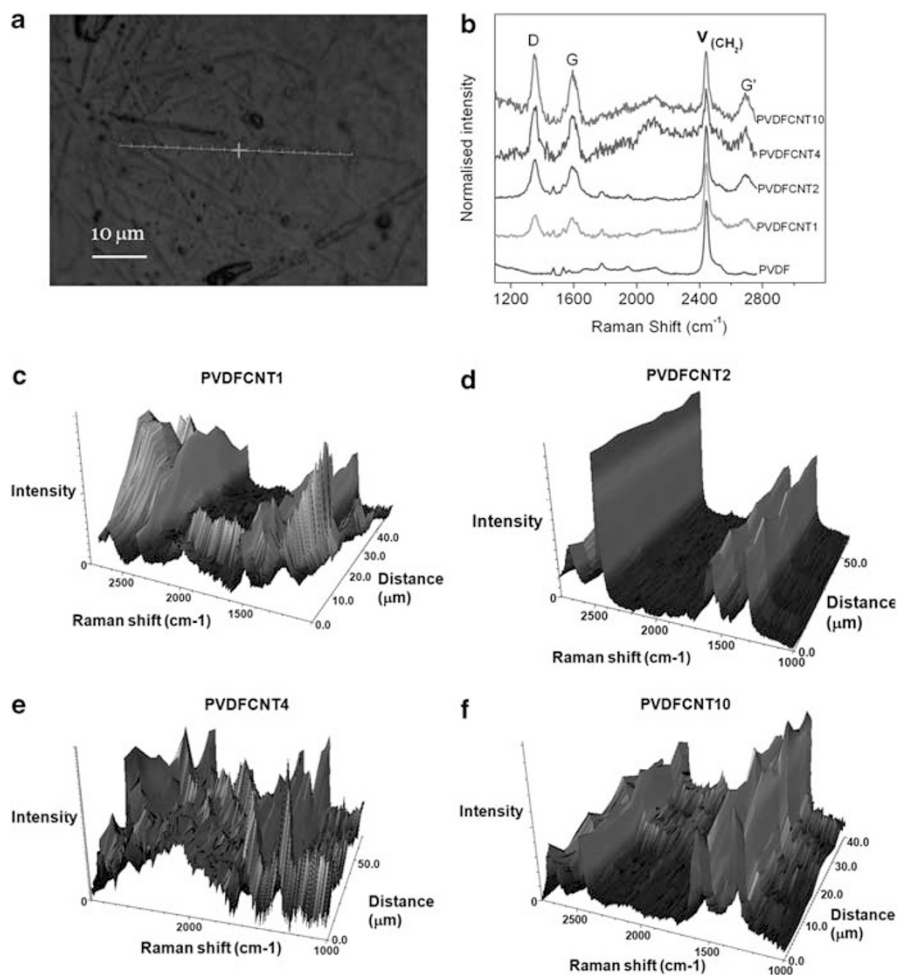
Figure 9 Raman spectra of PVDF/CNT composites using (**a**) line mapping to examine a large area of the sample. (**b**) The peaks arising from C-MWNTs (D-, G- and G'-bands) are indicated in normalized spectra. (**c**) Raman line mapping spectra acquired from positions along the line for PVDFCNT1, (**d**) PVDFCNT2, (**e**) PVDFCNT4 and (**f**) PVDFCNT10.

in the model through the annihilation of capacitive response for high concentrations. The model fits show the potential for this applied functionality in sensor deployment.

To understand the role of dispersion, we used Raman spectroscopy. As shown in Figure 9b, MWCNT peaks were found at 2700, 1590 and 1324 cm^{-1}. One of the intense peaks is the G-band of MWCNT at 1590 cm^{-1}, which is associated with several tangential C–C stretching transitions of MWCNT carbon atoms. Analyzing the intensity and location of these bands can be used to correlate the dispersion of nanotubes in the polymer matrix. The intense peak at 2470 cm^{-1} is associated with the PVDF band, which arises from C–H stretching. Peak intensities in Raman spectroscopy are proportional to the MWCNT concentration. Increases in the intensity and area of the G-, G'- and D-band peaks could be seen with increases in the concentration of MWCNT, which is consistent with the results reported by Salzmann *et al.*[36] Similarly, the PVDF band peak area decreased with an increase in MWCNT concentration. In Raman line mapping (Figures 9c, d, e and f), a multispectrum file is acquired. Each spectrum represents the Raman response of the composition present at the point at which the laser is focused. The image is obtained by integrating over all Raman lines. Using both images, the spectral data at different locations can be clearly linked to the distribution of MWCNT in the polymer matrix. When the G-band

was examined as a function of distance, it could be seen that low dispersion existed at 1% and corresponded to the least particle-to-particle contact and highest resistance. For 2 and 10%, well-dispersed particles were evident with periodic peaks and valleys that showed spatial uniformity (although with increased concentration, the period became smaller). For 4%, we detected agglomeration as the concentration transitioned from the absence of a particle-to-particle concentration to a continuous network.

CONCLUSIONS

A transition from NPC to PPC behavior for materials in compression was determined. The extent of PPC was related to the degree of particle-to-particle contact and was a function of material response. A novel transition from an electrically resistive to a conductive time-dependent response was determined in MWCNT-modified PVDF nanocomposites as a function of concentration. The magnitude of change in resistance was similar for high and low concentrations, indicating that resistivity-based piezoresponse can also be considered without requiring particle-to-particle contact in a non-piezoresponsive polymer. An electrical and mechanical analog for a time-dependent viscoelastic response was developed to describe the resistive response. The result from the model agreed well with the experimental data and offers the opportunity to make both an electrical and

mechanical time-dependent prediction in polymer-CNT nanocomposites. Raman spectroscopy was ideally suited for the investigation of MWCNT dispersion, as the laser probe could interrogate the large surface area. The results of this investigation show that a resistive piezoresponse is of value because the magnitude of the change in resistance, whether conductive or resistive, is a useful parameter in the correlation of stress effects.

ACKNOWLEDGEMENTS

1   Suhr, J., Koratkar, N., Keblinski, P. & Ajayan, P. Viscoelasticity in carbon nanotube composites. *Nat. Mater.* **4,** 134–137 (2005).
2   Ponomarenko, A., Shevchenko, V., Klason, C. & Pristupa, A. Magnetic-field-sensitive polymer composite materials. *Smart Mater. Struct.* **3,** 409–415 (1994).
3   Xia, H. & Wang, Q. Ultrasonic irradiation: a novel approach to prepare conductive polyaniline/nanocrystalline titanium oxide. *Chem. Mater.* **14,** 2158–2165 (2002).
4   Mei, Z., Guerrero, V., Kowalik, D. & Chung, D. Mechanical damage and strain in carbon fiber thermoplastic-matrix composite, sensed by electrical resistivity measurement. *Polym. Compos.* **23,** 425–432 (2002).
5   Yamaguchi, K., Busfield, J. & Thomas, A. Electrical and mechanical behavior of filled elastomers. I. The effect of strain. *J. Polym. Sci. B Polym. Phys.* **41,** 2079–2089 (2003).
6   Baughman, R., Cui, C., Zakhidov, A., Iqbal, Z., Barisci, J., Spinks, G., Wallace, G., Mazzoldi, A., De Rossi, D., Rinzler, A., Jaschinski, O., Roth, S. & Kertesz, M. Carbon nanotube actuators. *Science* **284,** 1340–1344 (1999).
7   Tahhan, M., Truong, V., Spinks, G. & Wallace, G. Carbon nanotube and polyaniline composite actuators. *Smart Mater. Struct.* **12,** 626–632 (2003).
8   Wood, J., Zhao, Q., Frogley, M., Meurs, E., Prins, A., Peijs, T., Dunstan, D. & Wagner, H. Carbon nanotubes: from molecular to macroscopic sensors. *Phys Rev. B.* **62,** 7571–7575 (2000).
9   Peng, S., O'Keeffe, J., Wei, C., Cho, K., Kong, J. & Chen, R. Carbon nanotube chemical and mechanical sensors. *Proceedings of the 3rd International Workshop on Structural Health Monitoring* Stanford, CA, pp 1–8 (2001).
10 Ajayan, P. & Zhou, O. in *Carbon Nanotubes Synthesis, Structure, Properties and Applications* (eds. Dresselhaus, M., Dresselhausand, G., Avouris, Ph.) *Applications of Carbon Nanotubes* pp 391–425 (2001).
11 Kang, I., Schulz, M., Kim, J., Shanov, V. & Shi, D. A carbon nanotube strain sensor for structural health monitoring. *Smart Mater. Struct.* **15,** 737–748 (2006).
12 Nam, Y., Kim, W., Cho, Y., Chae, D., Kim, G., Hong, S., Hwang, S. & Hong, S. Morphology and physical properties of binary blend based on PVDF and multi-walled carbon nanotube. *Macromol. Symp.* **249,** 478–484 (2007).
13 Song, Y., Zheng, Q. & Yi, X. Reversible nonlinear conduction in high-density polyethylene/acetylene carbon black composites at various ambient temperatures. *J. Polym. Sci. B Polym. Phys.* **42,** 1212–1217 (2004).
14 Xiao, M., Sun, L., Liu, J., Li, Y. & Gong, K. Synthesis and properties of polystyrene/graphite nanocomposites. *Polymer* **43,** 2245–2248 (2001).
15 Vipulanandan, C. & Garas, V. Electrical resistivity, pulse velocity, and compressive properties of carbon fiber-reinforced cement mortar. *J. Mater. Civil Eng.* **20,** 93–101 (2008).
16 Veedu, V., Cao, A., Li, X., Ma, K., Soldano, C., Kar, S., Ajayan, P. & Ghasemi-Nejhad, M. Multifunctional composites using reinforced laminae with carbon-nanotube forests. *Nat. Mater.* **5,** 457–462 (2006).
17 Sau, K., Khastgir, D. & Chaki, T. Electrical conductivity of carbon black and carbon fibre filled silicone rubber composites. *Die Angewandte Makromolekulare Chemie* **258,** 11–17 (1989).
18 Pramanik, P., Khastgir, D., De, S. & Saha, T. Pressure-sensitive electrically conductive nitrile rubber composites filled with particle carbon black and short carbon fiber. *J. Mater. Sci.* **25,** 3848–3853 (1990).
19 Baughman, R., Zakhidov, A. & Heer, W. Carbon nanotubes—the route toward applications. *Science* **297,** 787–792 (2002).
20 Qu, S. & Wong, S. Piezoresistive behavior of polymer reinforced by expanded graphite. *Compos. Sci. Technol.* **67,** 231–237 (2007).
21 Wu, M. & Shaw, L. Improved properties of injection-molded, carbon nanotube-filled PET/PVDF blends. *J. Power Sources* **136,** 37–44 (2004).
22 Taya, M., Kim, W. & Ono, K. Piezoresistivity of a short fiber/elastomer matrix composite. *Mech. Mat.* **28,** 53–59 (1998).
23 Mattmann, C., Clemens, F. & Troster, G. Sensor for measuring strain in textile. *Sensors* **8,** 3719–3732 (2008).
24 Wang, X. & Chung, D. Fiber breakage in polymer-matrix composite during static and fatigue loading, observed by electrical resistance measurement. *J. Mater. Res.* **14,** 4224–4229 (1999).
25 Zhang, X., Pan, Y., Zheng, Q. & Yi, X. Time dependence of piezoresistance for the conductor-filled polymer composites. *J. Polym. Sci. B* **38,** 2739–2749 (2000).
26 Dang, Z., Wu, J., Xu, H., Yao, S., Jiang, M. & Bai, J. Dielectric properties of upright carbon fiber filled poly (vinylidene fluoride) composite with low percolation threshold and weak temperature dependence. *Appl. Phys. Lett.* **91,** 072912 1–072912 3 (2007).
27 Kim, J., Loh, K. & Lynch, J. Piezoelectric polymeric thin films tuned by carbon nanotube fillers. *Proceedings of SPIE—15th Annual International Symposium on Smart Structures and Materials* 693232-1 (2008).
28 Laxminarayan, K. & Jalili, N. Functional nanotube-based textiles: pathway to next generation fabrics with enhanced sensing capabilities. *Text. Res. J.* **75,** 670–680 (2005).
29 Owens, F., Jayakody, J. & Greenbaum, S. Characterization of single walled carbon nanotube: polyvinylene difluoride composites. *Compos. Sci. Technol.* **66,** 1280–1284 (2006).
30 Zheng, Q., Zhou, J. & Song, Y. Time-dependent uniaxial piezoresistive behavior of high-density polyethylene/short carbon fiber conductive composites. *J. Mater. Res.* **19,** 2625–2634 (2004).
31 Chen, G., Lu, J., Lu, W., Wu, D. & Wu, C. Time-dependence of piezo-resistive behavior for polyethylene/foliated graphite nanocomposites. *Polym. Int.* **54,** 1689–1693 (2005).
32 Scotta, R. & Vitaliani, R. Structural dynamic and viscoelastic analysis via electric analogy. *J. Struct. Eng.* **122,** 1118–1121 (1996).
33 Liu, T. & Wang, X. Dynamic elastic modulus of single-walled carbon nanotubes in different thermal environments. *Phys. Lett. A* **365,** 144–148 (2007).
34 Fotheringham, D. & Cherry, B. Comment on the compression yield behaviour of polymethyl methacrylate over a wide range of temperatures and strain-rates. *Mater. Sci. Lett.* **11,** 1368–1371 (1976).
35 Matsumura, M. & Hirose, Y. Negative-capacitance effect in forward-biased metal oxide semiconductor tunnel diodes (MOSTD). *Jpn. J. Appl. Phys.* **39,** L123–L125 (2000).
36 Salzmann, C., Chu, B., Tobias, G., Llewellyn, S. & Green, M. Quantitative assessment of carbon nanotube dispersions by raman spectroscopy. *Carbon* **45,** 907 (2007).